

Supporting information

Reversible pH-Induced Fluorescence Colour Change of Gold Nanoclusters Based on pH-Regulated Surface Interactions

Daniel Cuaran-Acosta,[†]Pablo Londoño-Larrea,[†]Elena Zaballos-García,^{†,*} Julia Pérez-Prieto^{‡,*}

[†] Departamento de Química Orgánica, Universidad de Valencia, Av. VicentAndres Estelles s/n, 46100, Burjassot (Spain)

[‡] Instituto de Ciencia Molecular (ICMol), Universidad de Valencia, Catedrático José Beltrán 2, 46980, Paterna, Valencia (Spain).

***E-mail: julia.perez@uv.es**

Table of Contents

1. Experimental section	Page S3-S4
2. Additional figures and tables	Page S5
3. Estimate of NAD ⁺ molecules per AuNC	Page S8-S10
4. Study of the reversibility of the pH sensing	Page S11
5. Comparison between the performances of AuNC@NAD with that of other metal nanoclusters and BODIPYs	Page S18

1. Experimental Section

Materials and Methods. All chemicals used were of analytical grade. Nicotinamide adenine dinucleotide (NAD⁺), (2-Hydroxyethyl)-1-piperazineethanesulfonic acid sodium salt (HEPES-Na), gold (III) chloride trihydrate (HAuCl₄·3H₂O), sodium hydroxide (NaOH), chloroform, hydrochloric (HCl), were purchased from Sigma-Aldrich. All other reagents were of analytical reagent grade and were used as received. In all cases the glassware used in the following procedures was cleaned in a bath of freshly prepared solution of HNO₃–HCl (1:3, v/v) and rinsed thoroughly in water prior to use. For all aqueous solutions, high purity deionized water from Millipore system was used. AuNP@NAD⁺ solutions were centrifuged at 19,000 rpm (33,020 x g) for 30 min. in an Optima Max Ultracentrifuge with MLA-130 Rotor. The supernatant was collected with care to avoid disturbing the red precipitate.

UV/vis absorption spectra were recorded on an Agilent 8453E spectrophotometer. All the data were acquired using 1cm×1cm path length quartz cuvettes. Fluorescence spectra were taken in an Aminco Bowman Series 2 Luminescence spectrophotometer, equipped with a lamp power supply and working at room temperature. The AB2 software (v.25 5.5) was used to register the data. The quantum yields were measured with a Hamamatsu C9920-02 absolute PL Quantum Yield Measurement System. Time-resolved photoluminescence decays were measured using a Compact fluorescence lifetime spectrometer C11367, Quantaurus-Tau, with seven types of LED light source (280 nm, 340 nm, 365 nm, 405 nm, 470 nm, 590 nm, 630 nm). This equipment permits fluorescent lifetime measurement with single-photon-counting sensitivity. Fluorescence lifetime measurement software U11487 was used to register the data. The PL decay data of the AuNCs dispersed in water were acquired using 1cm×1cm path length quartz cuvettes, and at excitation wavelengths are specified in Table S4. The PL decays of the nanoclusters were fitted with a triexponential function of time (*t*) equation 1, where τ_i are the decay times and α_i represents the amplitudes of the components.

$$I(t) = \sum_i \alpha_i \left(-\frac{t}{\tau_i} \right)$$

Structural and morphological characterizations of AuNC@NAD⁺ were performed using bright field transmission electron microscopy (TEM) JEOL JEM-1011 and high resolution TEM (HRTEM). A field emission gun (FEG) TECNAI G2 F20 microscope, operated at 200 kV, was used. Samples were deposited on carbon films 72 hours prior to measurement in each of the means of dispersion and dried in a vacuum. The diameter of the nanoparticles was determined by ImageJ, in nanometres. Statistical analysis was obtained by measuring the diameter value of 220 nanoparticles. X-ray photoelectron spectroscopy (XPS, K-ALPHA, Thermo Scientific) was used to analyze the samples surface. All spectra were collected using Al-K_α radiation (1486.6 eV), monochromatized by a twin crystal monochromator, yielding a focused X-ray spot (elliptical in shape with a major axis length of 400 μm) at 3 mA × 12 kV. The alpha hemispherical analyzer was operated in the constant energy mode with survey scan pass energies of 200 eV to measure the whole energy band and 50 eV in a narrow scan to selectively measure the particular elements. AuNC@NAD samples were digested in a microwave oven at 200 ° C with 100 μL of HNO₃: HCl 1:1 and ultrapure water was added to bring them up to the final volume. The determination of gold was performed by ICP-MS in Helio mode, in an Agilent model 7900, using iridium as the internal standard. The ¹H and ³¹P NMR spectrum were registered at room temperature in a Bruker DPX400 spectrometer, with a 400 MHz Bruker magnet. The chemical shifts (δ) are reported in ppm using deuterium oxide, 99.9% atom (D₂O) as solvent.

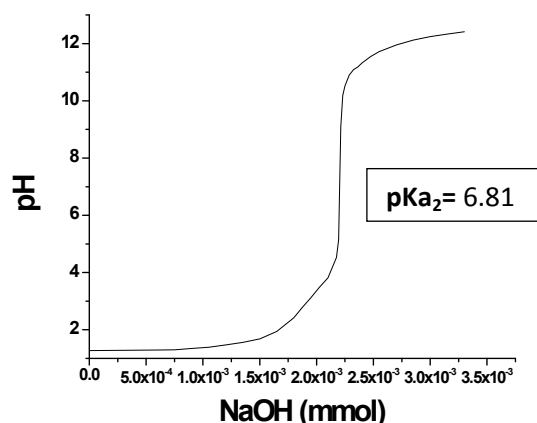


Figure S1. Titration curve of NAD⁺

Synthesis of AuNC@NAD⁺. Colloidal AuNCs were prepared by a top-down strategy based on the reduction of Au ions in the presence of a reducing agent like HEPES-Na and a functional organic ligand, specifically NAD⁺. Figure S2(top) shows a schematic representation of the steps followed for the synthesis of AuNC@NAD⁺ nanoclusters: a slow reduction of HAuCl₄ to form AuNPs (step 1); disaggregation of the AuNPs by adding NaOH (step 2); etching of the plasmonic nanoparticles by addition of HCl to generate intense fluorescent AuNCs (step 3). A 15 mL volumetric falcon flask was filled with reagents in the following order: chloroform (5 mL), a freshly prepared aqueous solution of HAuCl₄ (50 μ L, 50 mM) and an aqueous solution of HEPES-Na (1 mL, 10 mM, pH=8). Fast fading of the light yellow aqueous solution was observed. Then a NAD⁺ aqueous solution (80 μ L, 50 mM) was added and the mixture was stirred at 25 $^{\circ}$ C for 5 minutes to obtain a violet dispersion of AuNPs (AuNP@NAD⁺). This aqueous solution was separated from the chloroform by decantation and it turned red when mixed with aqueous NaOH (30 μ L, 2M). The AuNPs were centrifuged at 19000 RPM (33020 g) for 30 minutes. HCl (80 μ L, 2M) was added to the red precipitate. The blue supernatant gradually turned light gray (AuNC@NAD⁺). After centrifugation, the transparent, colourless colloid exhibited high blue luminescence under $\lambda_{exc} = 365$ nm. Figure S2 (bottom) compares the spectra of the plasmonic AuNPs and the AuNCs.

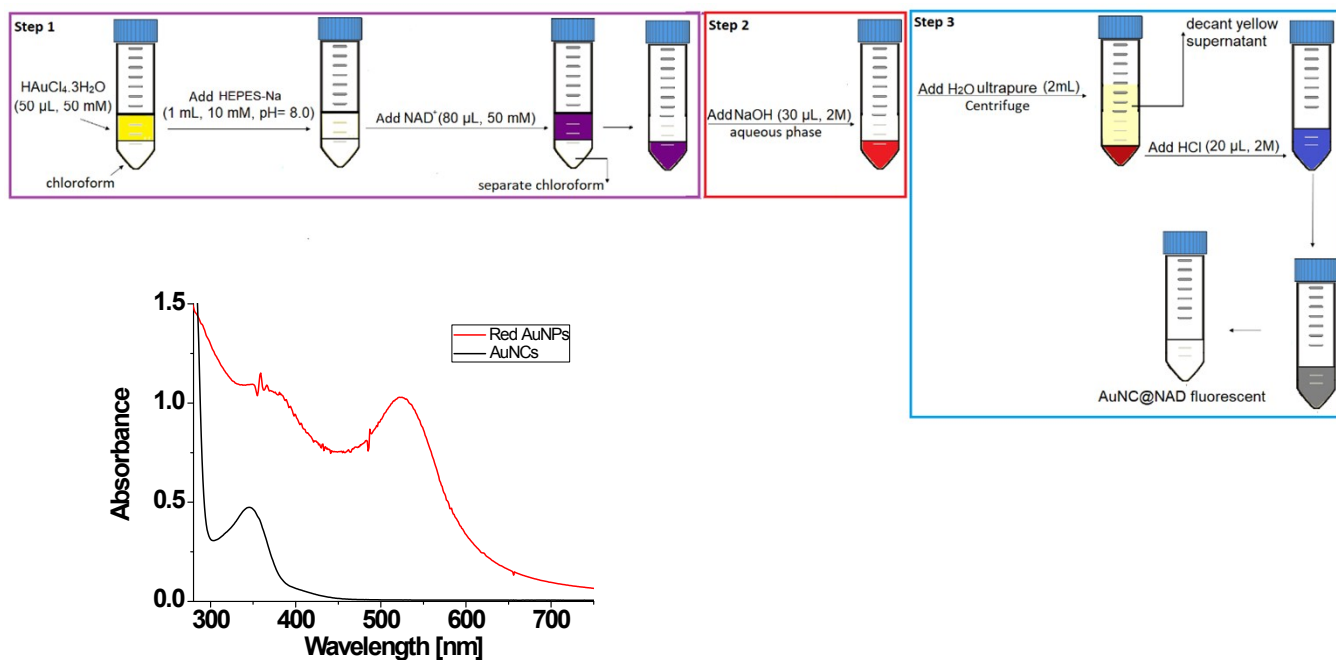


Figure S2. Top: Schematic representation of the three-step process for the synthesis of the water dispersible AuNC@NAD⁺ colloid. Bottom: comparison between the absorption spectra of the red water dispersible AuNP colloid (step 2) and the colourless AuNC@NAD⁺ colloid.

2. Additional figures and tables

The integration of the ^1H NMR spectrum of NAD^+ (Figure S3a, top) shows a 3:3 ratio between the signals in the 9.5 - 9.0 ppm range and those in the 8.9 - 8.0 ppm range, which are ascribed to the six aromatic protons of the adenine and nicotinamide. That ratio is preserved in the spectrum of AuNC@NAD (Figure S3a, bottom), thus ruling out the reduction of the NAD^+ moiety to NADH . Table S1 compares relevant signals of NAD^+ and NADH .

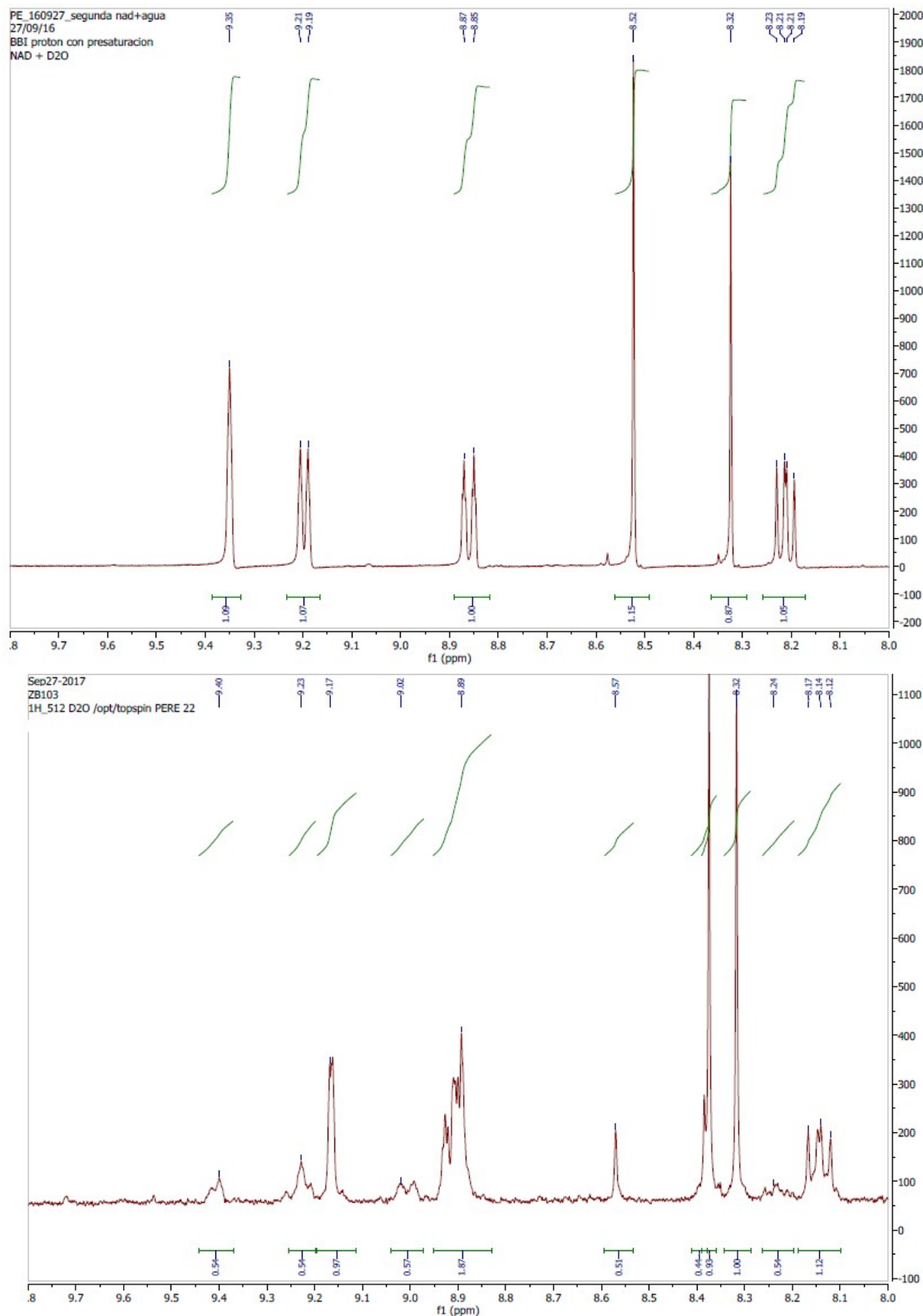


Figure S3a. Comparison between the ^1H NMR spectra of NAD^+ (top) and AuNC@NAD (bottom) in the 6.9-9.4 ppm region.

Table S1. Comparison between the $^1\text{H-NMR}$ signals of nicotinamide and adenine in the 6.9-9.4 ppm region.

	NAD⁺^a	NADH²^a
Nicotinamide-C-2-H	9.32	6.98
Nicotinamide-C-6-H	9.17	-
Nicotinamide-C-4-H	8.84	2.8
Adenine-C-8-H	8.41	8.45
Adenine-C-2-H	8.11	8.20
Nicotinamide-C-5-H	8.21	-

^aX. Huang, I.H El-Sayed, X. Yi, M.A El-Sayed. Gold nanoparticles: Catalyst for the oxidation of NADH to NAD⁺. *Journal of Photochemistry and Photobiology B: Biology*, 2005, **81**, 76-83; W.A. Catterall, D.P. Hollis, C.F. Walter, Nuclear magnetic resonance studies on pyridine dinucleotides: The pH dependence of the carbon-13 nuclear magnetic resonance of NAD⁺ analogs. *Biochemistry* 1969, **8**, 4032–4036.

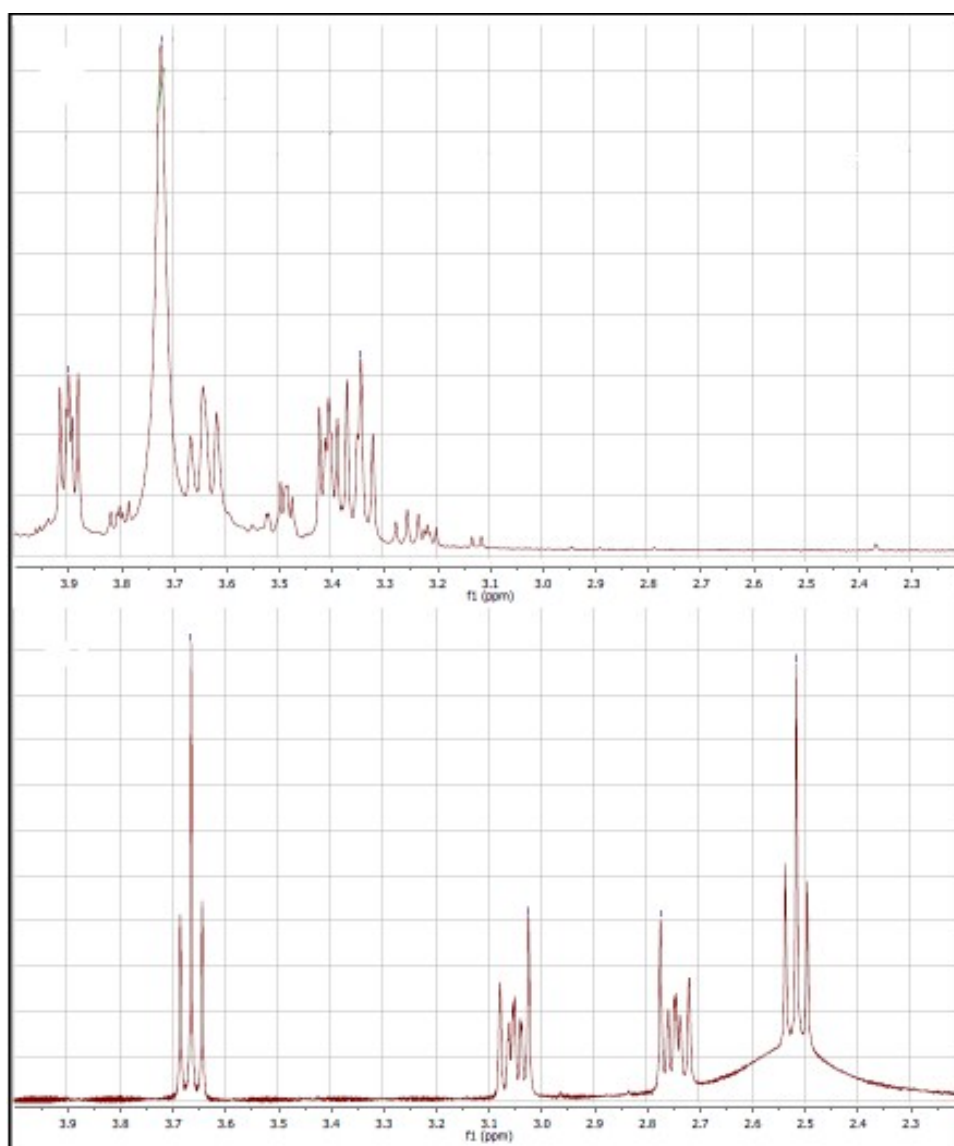


Fig. S3b shows the comparison between the colloidal sample (top) and that of free HEPES (bottom). The most significant variations were the displacement of the signals in the NC and their widening in i) the 3.65 – 2.4 ppm zone with respect to those of HEPES and ii) the 9.5-8.1 zone with respect to those of NAD⁺ (nicotinamide and adenine aromatic rings). The widening of the signals in AuNC@NAD⁺ is consistent with the restricted movement of the ligands within the organic capping of the NC.

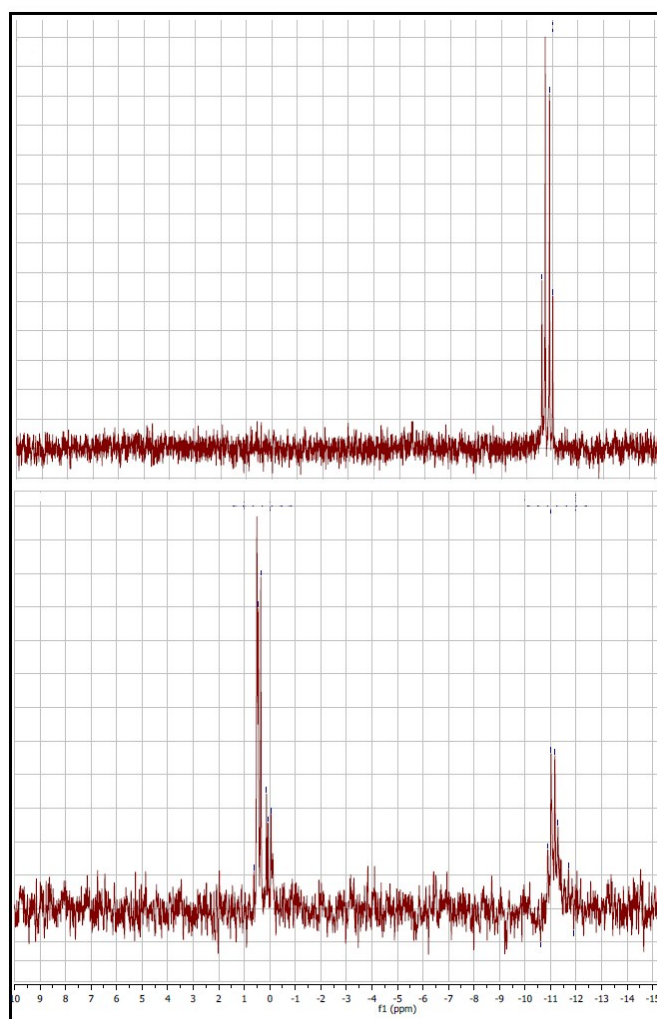


Figure S4. Comparison between the ^{31}P NMR spectra of NAD^+ (top) and AuNC@NAD^+ (bottom).

Time-resolved photoluminescence studies

Table S2. Lifetime data of the photoluminescence of AuNC@NAD $\lambda_{\text{emi}}: 430\text{nm}$

λ_{exc}	CHI	$\tau_{\text{av}}(\text{ns})$	$\tau_1(\text{A1})$	$\tau_2(\text{A2})$	$\tau_3(\text{A3})$
340 nm	1.146	4.01	0.002 (15.6%)	3.67 (63.3%)	4.78 (21.1%)
365 nm	1.026	4.12	1.43 (19.1%)	3.62 (68.9%)	6.60 (12.0%)

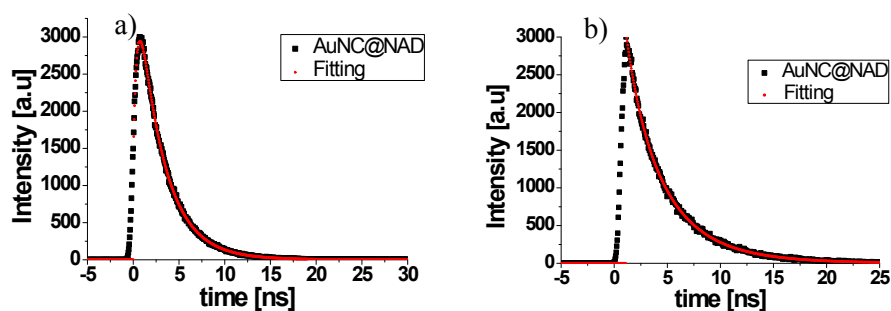


Figure S5. Kinetic traces of the photoluminescence of AuNC@NAD^+ at $\lambda_{\text{em}} 418\text{ nm}$: $\lambda_{\text{exc}} 340\text{ nm}$ (left) and $\lambda_{\text{exc}} 365\text{ nm}$ (right).

High-resolution transmission electron microscopy images. Figure S6 shows the formation of AuNC@NAD⁺ of 2.09 ± 0.37 nm in diameter. The 0.21 nm distance between planes corresponds to the (200) plane of the cubic phase structure of Au (JCPDS file 01-075-6560).

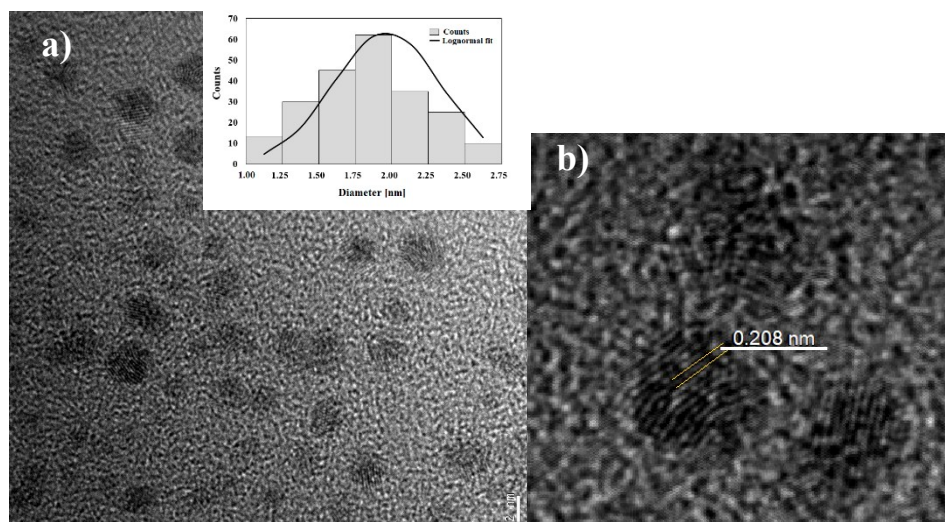


Figure S6. a) HRTEM image of AuNC@NAD⁺ and histogram with the nanocluster-size distribution. Statistical analysis was obtained by measuring the diameter of 220 nanoclusters; b) HRTEM image of AuNC@NAD⁺ showing the characteristic distance between planes of Au.

The X-ray photoelectron spectrum (XPS) of AuNC@NAD⁺ was consistent with the presence of HEPES and NAD⁺. The XPS of P showed the 2p_{3/2} and 2p_{1/2} bands with binding energies (BEs) of 133.00 eV and 134.30 eV, respectively. The XPS of S showed the 2p_{3/2} and 2p_{1/2} bands with BEs of 167.68 eV and 168.88 eV, respectively (Figure S7).

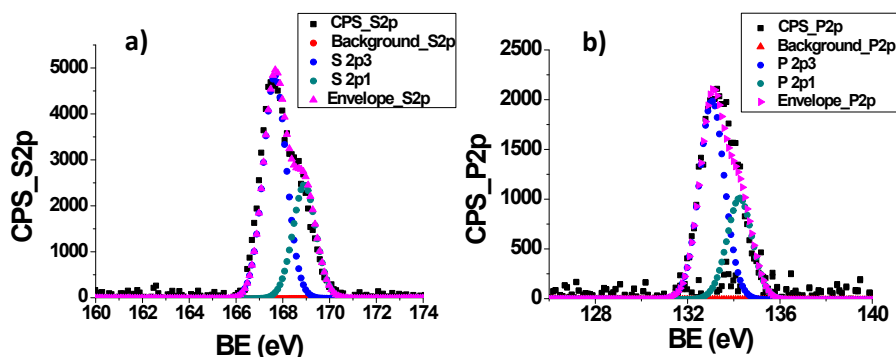


Figure S7. XPS spectra of AuNC@NAD: S 2p (a), and P 2p (b).

3. Estimate of NAD⁺ molecules per AuNC

Table S3. ICP-MS Results

Au	[Au] calculated by ICP-MS	Volume (mL)	Au (mg)
Au in AuNC@NAD ⁺	92.0 mg/L	14 mL	1.3 mg
Au in the yellow supernatant	103.0 mg/L	270 mL	27.8 mg

Content of Au and NAD⁺ ligand in the nanoclusters

Surface area of the sphere (nm²)

$$4\pi r^2 = 4\pi \left(\left(\frac{2.1}{2} \right) - (0.145) \right)^2 = 10.2 \text{ nm}^2$$

Where:

0.145 = Radius of a gold atom.

Number of Au atoms on the surface

$$\text{Number of Au atoms} = \rho * A$$

Where:

$$\rho = 13,89 \frac{\text{atoms}}{\text{nm}^2}; \text{ surface density of the gold atoms (Au)}$$

A = Surface area of the sphere (nm²)

$$13,89 \frac{\text{atoms}}{\text{nm}^2} * 10.2 \text{ nm}^2 = 141.4 \text{ atoms Au}$$

Volume of the sphere (nm³)

$$\frac{4}{3}\pi r^3 = \frac{4}{3}\pi \left(\left(\frac{2.1}{2} \right) \right)^3 = 4.8 \text{ nm}^3$$

Number of Au atoms forming the sphere

$$\text{Number of Au atoms} = \rho * V$$

Where:

$$\rho = 58,01 \frac{\text{atoms}}{\text{nm}^3}; \text{ volumetric density of the gold atoms}$$

V = volume of the sphere (nm³)

$$58,01 \frac{\text{atoms}}{\text{nm}^3} * 4.8 \text{ nm}^3 = 277.3 \text{ atoms Au}$$

Number of Au atoms in the nanocluster

Total number of Au atoms = Number of atoms on surface + Number of atoms forming the sphere.

$$141.4 \text{ atoms Au} + 277.3 \text{ atoms Au} = 418.7 \text{ atoms Au}$$

Moles of Au/nanocluster

$$418.7 \text{ atoms Au} \times \frac{1 \text{ mol Au}}{6.022 \times 10^{23} \text{ atoms Au}} = 6.9 \times 10^{-22} \text{ moles Au}$$

From the total number of Au atoms per nanocluster and with the total amount of Au obtained according to the results of ICP-MS, the total number of nanoclusters obtained can be estimated:

Total moles of Au (according to ICP-MS)

$$\frac{92 \text{ mg}}{1000 \text{ mL}} \times 14 \text{ mL} = 1.3 \text{ mg Au}$$

$$1.3 \text{ mg Au} \times \frac{1 \text{ mmol Au}}{196.97 \text{ mg Au}} = 6.5 \times 10^{-6} \text{ moles Au}$$

Number of AuNCs

$$6.5 \times 10^{-6} \text{ moles Au totales} \times \frac{\text{Nanocluster}}{6.9 \times 10^{-22} \text{ moles Au}} = 9.4 \times 10^{15} \text{ NCs}$$

Moles of nanoclusters

$$9.4 \times 10^{15} \text{ Nc} \times \frac{1 \text{ mol NC}}{6.022 \times 10^{23}} = 1.6 \times 10^{-8} \text{ moles NC}$$

Calculation of NAD⁺ bound to surface of NCs. ICP-MS analysis was used to estimate the amount of NAD⁺ and quantify the number of phosphors in the sample, since the NAD⁺ is the only compound in the NC with phosphorus in its structure.

Calculation of the phosphorus (P) amount

$$\frac{49.7 \text{ mg P}}{1000 \text{ mL}} \times 14 \text{ mL} = 0.7 \text{ mg P}$$

Calculation of NAD⁺ moles

$$0.7 \text{ mg P} \times \frac{1 \text{ mmol P}}{30.98 \text{ mg P}} \times \frac{1 \text{ mmol NAD}^+}{2 \text{ mmol P}} = 1.1 \times 10^{-5} \text{ moles NAD}^+$$

$1.1 \times 10^{-5} \text{ moles NAD}^+ / 1.6 \times 10^{-8} \text{ moles Nc} = \text{ca. } 718 \text{ molecules NAD}^+/\text{NC}$
--

4. Study of the reversibility of the pH sensing

Reagents: NaOH 1 M (p), HCl 1M (a).

AuNC@NAD⁺ at pH 1 → 12 and AuNC@NAD⁺ at pH 12 → 1

Twelve NaOH aliquots (20 μL, 1 M) were added to 200 μL of the aqueous colloid of AuNC@NAD⁺, initially at pH 1. The spectrum of the colloid was recorded after each addition and compared with that of the initial colloid. Similarly, twelve HCl aliquots (20 μL, 1 M) were added to 200 μL of the aqueous colloid of AuNC@NAD⁺, initially at pH 12. The spectrum of the colloid was recorded after each addition and compared with that of the initial colloid (Figure S8).

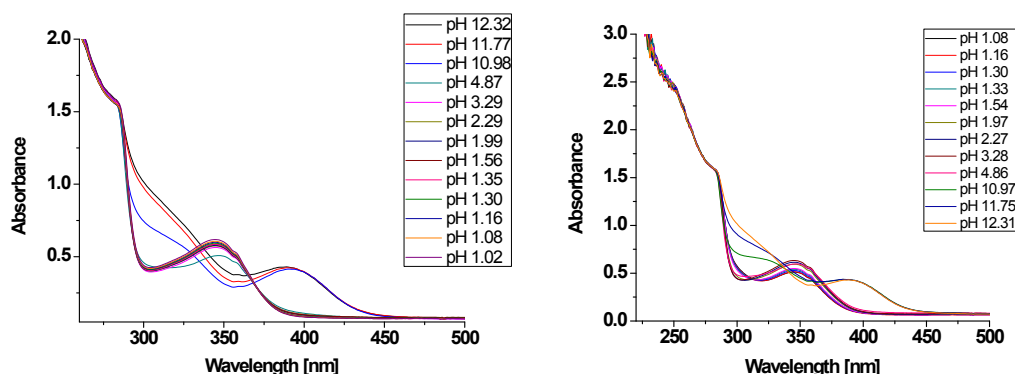


Figure S8. Evolution of the UV spectrum of AuNC@NAD⁺ from pH 1 to pH 12 by addition of NaOH aliquots and from pH 12 to pH 1 by addition of HCl aliquots.

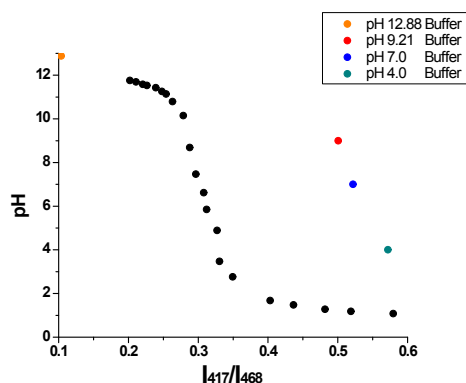


Figure S9. Comparison between the response of the I_{417}/I_{468} ratio of the AuNCs to different pHs using commercially available buffers and the ratiometric curve determined by using increasing NaOH mmol. It shows the similar dependence of the I_{417}/I_{468} ratio on the pH at the linear interval, though the I_{417}/I_{468} values were different. Buffers pH 4.01 (potassium hydrogen phthalate), pH 7.00 (potassium and disodium phosphate), and pH 9.21 (Borax) contain germicide; buffer at 12.88 was prepared by using HEPES-Na (10mM, 5 mL) plus NaOH (1M, 1 mL).

-AuNC@NAD⁺ Size (acid medium)
2.09 ± 0.37 nm

-AuNC@NAD⁺ Size (basic medium)
2.05 ± 0.44 nm

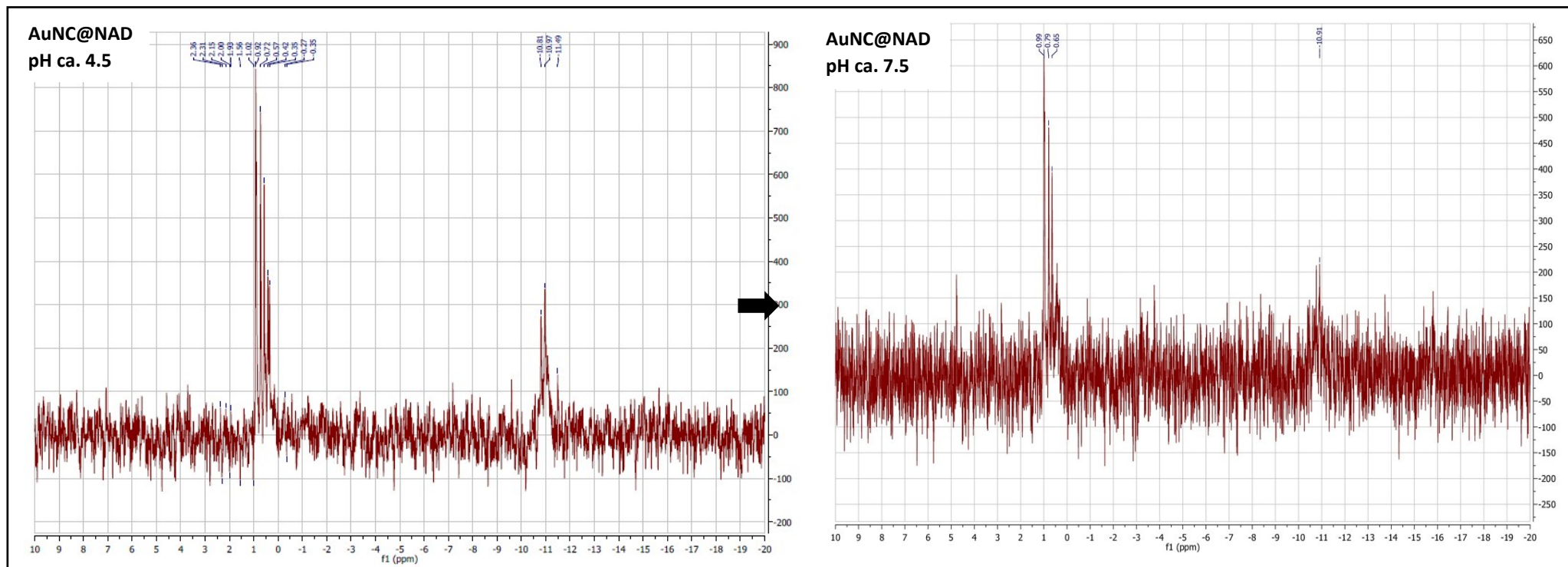


Figure S12. ^{31}P NMR spectrum of AuNC@NAD⁺ at pH ca. 4.5 and 7.5.

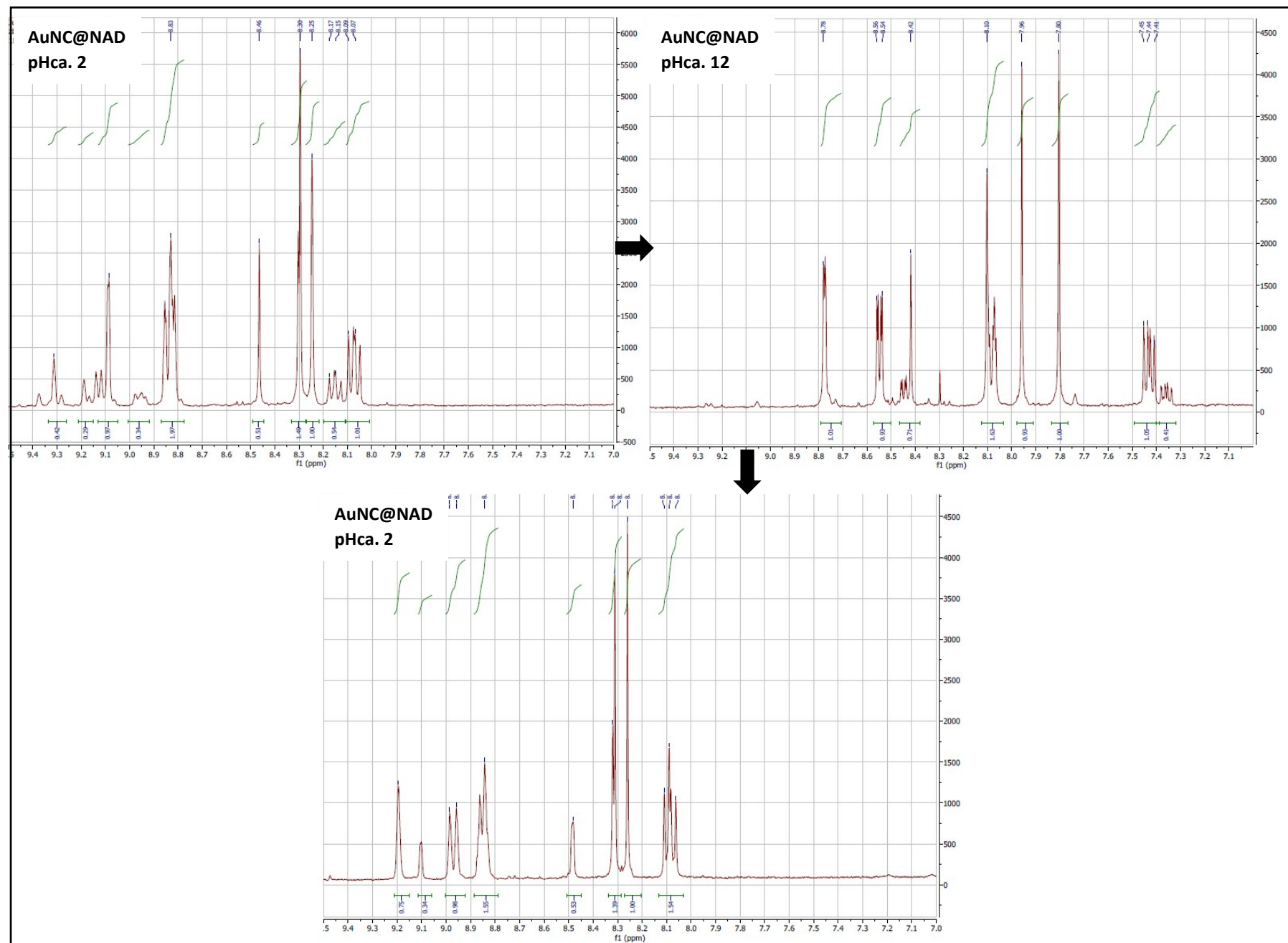


Figure S13. Evolution of the ^1H NMR spectrum of AuNC@NAD⁺ at pH 2 after treatment with NaOH up to pH 12 followed by treatment with HCl down to pH 2.

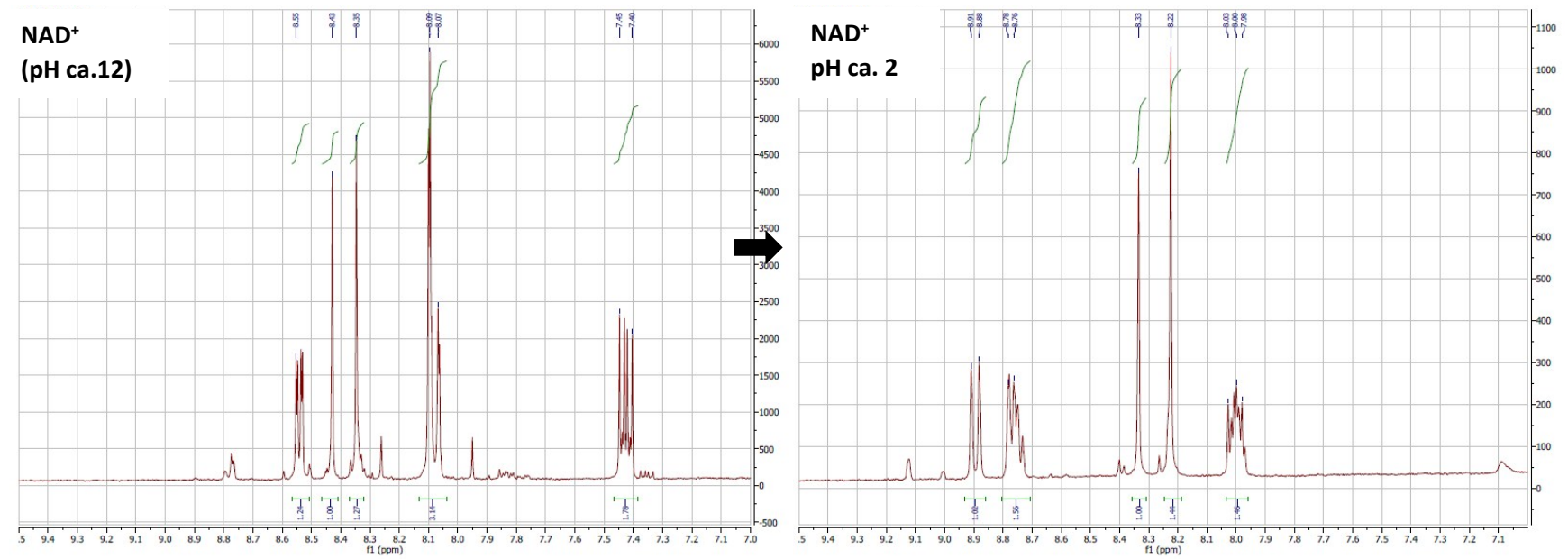
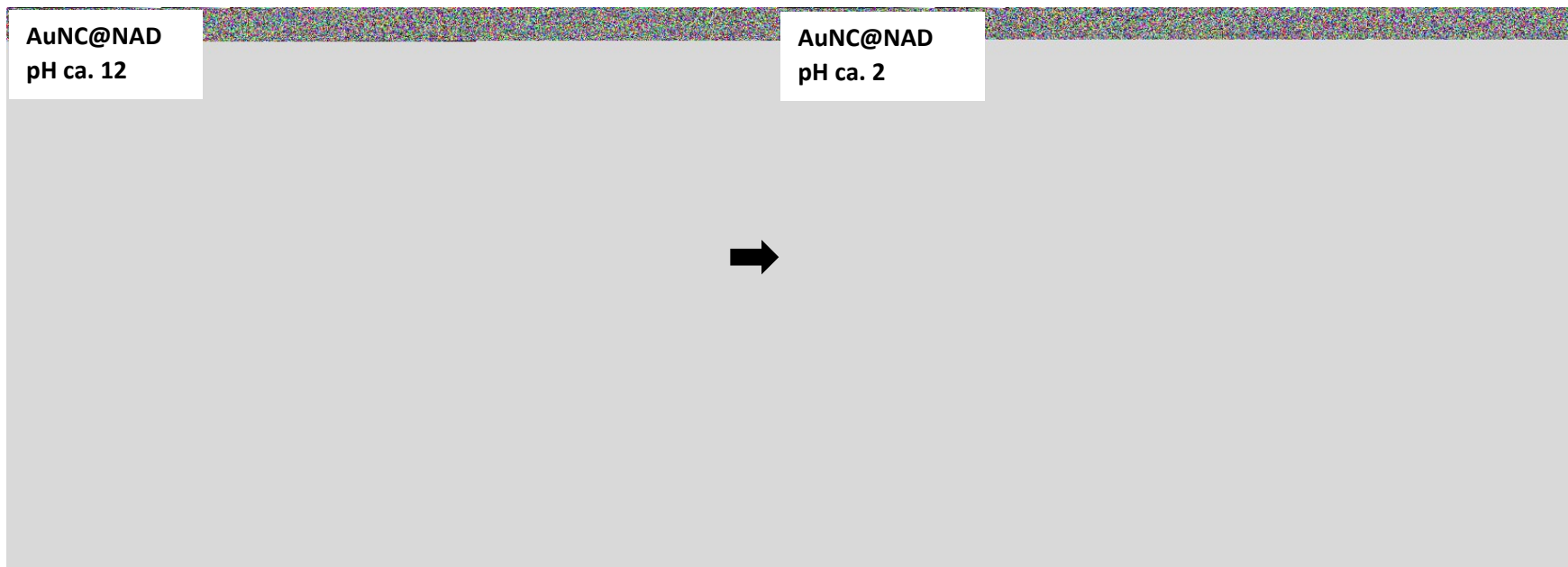


Figure S14. ¹H NMR spectra of AuNC@NAD⁺ and NAD⁺ at pH 12 and those after treatment with NaOH down to pH 2, showing the instability of NAD⁺ at pH 12

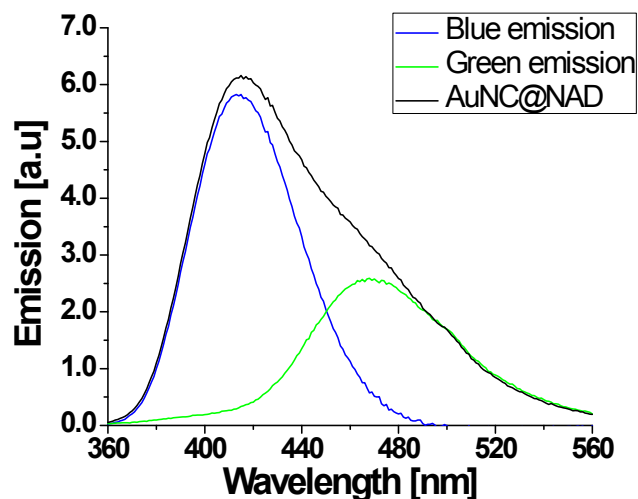


Figure S15. Spectra of the blue emission of the AuNC@NAD⁺ nanoclusters (in blue) obtained by subtraction of the green emission of the nanocluster in basic medium (spectrum in Figure 1b₄) from the emission of the nanoclusters at acid medium (Figure 1 b₃).

Table S4. Comparison between the photoluminescence lifetime and quantum yield of AuNC@NAD at two extreme pHs

AuNC@NAD ⁺ pH 1 $\lambda_{em}:430$ nm						AuNC@NAD ⁺ pH 12 $\lambda_{em}:470$ nm					
-Lifetime measurement						-Lifetime measurement					
λ_{exc}	CHI	τ_{av} ns	τ_1 (A1)	τ_2 (A2)	τ_3 (A3)	λ_{exc}	CHI	τ_{av} ns	τ_1 (A1)	τ_2 (A2)	τ_3 (A3)
340 nm	1.146	4.01	0.002 (15.6%)	3.67 (63.3%)	4.78 (21.1%)	365 nm	1.036	4.59	0.018 (83.1%)	1.18 (7.5%)	5.2 (9.4%)
365 nm	1.026	4.12	1.43 (19.1%)	3.62 (68.9%)	6.60 (12.0%)	405 nm	1.167	4.73	6×10^{-6} (78.2%)	1.41 (6.8%)	5.14 (15%)
-Quantum yield ($\lambda_{exc} = 350$ nm) $\Phi_{PL} = 22.8$ %						-Quantum yield ($\lambda_{exc} = 400$ nm) $\Phi_{PL} = 20.4$ %					

5. Comparison between the performances of AuNC@NAD with that of other metal nanoclusters and BODIPYs

Table S5. Comparison between the performances of AuNC@NAD with that of other metal nanoclusters reported in the literature

	AuNC@NAD ^a	AgNCs capped by hyperbranched polyethyleneimine ^a	Polyethyleneimine-protected CuNCs ^b	Copper nanoclusters ^c	PEGylate porphyrin-AuNCs ^d
λ_{em} (λ_{exc})	417nm (350 nm) 468nm (395 nm)	455nm (375 nm)	495nm (380nm)	417nm (337nm)	654 nm (424nm)
Fluorescence color	pH < 7, blue pH > 7, green	pH > 8, blue pH < 5, colorless	pH > 6, blue pH < 5, colorless	pH > 6, blue	red
pH responsive linear range	3.0 – 11.0	4.10 – 7.96; 4.78 – 7.96; 6.09 – 8.95	-	6.1 – 12.1	1.0 – 6.0
Quantum yield (λ_{exc})	22.8 % (350 nm) 20.4 % (400 nm)	-	7.5 %	-	-
Lifetime (λ_{exc})	4.01 ns (340 nm) 4.12 ns (365nm)	-	5.70 ns	3.98 ns	-
Stability	6 months	-	-	2 months	2 months
Reversibility	9 cycles (1.0 – 12.0)	-	-	5 cycles (6.2– 1.8)	5 cycles (1.0 – 6.0)

*Nanoclusters reported in this MS

^aF. Qu, X. Zou, R. Kong, J. You. A tunable pH-sensing system based on Ag nanoclusters capped by hyperbranched polyethyleneimine with different molecular weights. *Talanta*, 2016, **146**, 549-555.

^bC. Wang, Y. Yao, Q. Song. Interfacial synthesis of polyethyleneimine-protected copper nanoclusters: Size-dependent tunable photoluminescence, pH sensor and bioimaging. *Colloids and Surfaces B: Biointerfaces*, 2016, **140**, 373–381.

^cY. Qiao, T. Xu, Y. Zhang, C. Zhang, L. Shi, G. Zhang, S. Shuang, C. Dong. Green synthesis of fluorescent copper nanoclusters for reversible pH-sensors. *Sensors and Actuators B*, 2015, **220**, 1064-1069.

^dP.GMineo, A. Abbadessa, A. Rescifina, A. Mazzaglia, A. Nicosia, A.A Scamporrino. PEGylate porphyrin-gold nanoparticles conjugates as removable pH-sensor nano-probes for acidic environments. *Colloids and Surfaces A*, 2018, **546**, 40–47.

Table S6. Comparison between some features of AuNC@NAD⁺ and those of some BODIPYs reported in the literature.

	AuNC@NAD ⁺	BODIPYs ^a	AIE-based BODIPYs ^b	bis(methoxycarbonyl)ethenyl functionalized BODIPY ^c	Benzimidazole-BODIPY ^d
λ_{em} (λ_{exc})	417nm (350 nm) 468nm (395 nm)	530 nm (~ 500 nm)	470 nm (370 nm)	603 nm – 611 nm (570 nm)	560 nm (505 nm)
Fluorescence color	pH < 7: Blue fluorescence pH>7: Green fluorescence	pH < 8: Green fluorescence pH > 8: No fluorescence	pH 5.0 – 9.0: Green fluorescence pH > 10.0: No fluorescence	Red fluorescence	Acid green Fluorescence Basic No fluorescence
pH responsive linear range	3.0 – 11.0	5.0 – 12.0	7.0 – 11.0	3.0 – 10.0	-
Quantum yield	350 nm: 22.8 % 400 nm: 20.4 %	475 nm >50%, up to 90%	-	45 % - 76 %	57 %
Lifetime	340nm: 4.01 ns 365nm: 4.12 ns	2.97 – 6.58 ns	-	-	-
Stability	6 months	-	-	-	-
Reversibility	9 cycles (1.0 – 12.0)	-	5 cycles (7.0 – 11.0)	-	-

* Nanoclusters reported in this MS

a S. Radunz, H. Rune-Tschiche, D. Modenhauer, U. Resch-Genger. Broad range ON/OFF pH sensors based on pKa tunable fluorescent BODIPYs. *Sensors and Actuators B: Chemical*, 2017, **251**, 490-494.

b J. Qiu, S. Jiang, H. Guo, F. Yang. An AIE and FRET-based BODIPY sensor with large Stoke shift: Novel pH probe exhibiting application in CO₃²⁻ detection and living cell imaging. *Dyes and Pigments*, 2018, **157**, 351-358.

c E. Teknikel, C. Unaleroglu. Colorimetric and fluorometric pH sensor based on bis(methoxycarbonyl)ethenyl functionalized BODIPY. *Dyes and Pigments*, 2015, **120**, 239-244.

d Z. Li, L. Li, T. Sun, L. Liu, Z. Xie. Benzimidazole-BODIPY as optical and fluorometric pH sensor *Dyes and Pigments*, 2016, **128**, 165-169.